Volume 10, Issue 2, 2020, 5076 - 5084 ISSN 2069-5837
Biointerface Research in Applied Chemistry
www.BiointerfaceResearch.com
https://doi.org/10.33263/BRIAC102.076084
Original Research Article Open Access Journal
Received: 09.12.2019 / Revised: 18.01.2020 / Accepted: 25.01.2020 / Published on-line: 27.012020

Diffusion & concentration effect of Li/Li$^+$ to the efficiency of LIBs

Chanh Minh Thi Le [1, 2], Majid Monajjemi [1, 3, *], Thu Thi Pham[1], Fatemeh Mollaamin [1], Chien Mau Dang [1, *]

[1]Institute for Nanotechnology (INT)– Vietnam National University - Ho Chi Minh city Community 6, Linh Trung Ward, Thu Duc District, Ho Chi Minh City, 700000, Vietnam
[2]University of Science – Vietnam National University - Ho Chi Minh City 227 Nguyen Van Cu Street, ward 4, district 5, Ho Chi Minh City, 700000, Vietnam
[3]Department of chemical engineering, Central Tehran Branch, Islamic Azad University, Tehran, Iran
*corresponding author e-mail address: ***dmchien@yahoo.com; maj.monajjemi@iauctb.ac.ir*** Scopus ID 54406655100; 6701810683

ABSTRACT

In this work the concentration of Li/Li+ has applied for increasing the efficiency of Lithium ion batteries. Various numbers of lithium and lithium cations have been simulated as diffused atoms in graphite as anode materials. We have found the structure of (G// (h-BN) //G) can be to improve the voltage and electrical transport in anodic sheets-based LIBs. This system could also be assembled into free-standing electrodes without any binder or current collector, which will lead to increased specific energy density for the overall battery design. Therefore, the above modification of BN-G sheet and designing of this kind structure provide strategies for improving the performance of material based anodes in LIBs.

Keywords: *lithium ion battery; graphene doped electrodes; h-BN sheet.*

1. INTRODUCTION

Lithium ion batteries (LIBs) are significant energy storage devices based on electrochemical energy, widely used in a small storage system. With the discovery of highly reversible, Li-intercalation carbonaceous materials and low-voltage battery, Sony realized the commercialization of xC6/Li $_{1-x}$ CoO_2 cells in 1991 [1]. Although the electrolyte establishes high ionic conductivity between two electrodes, the electrolytes are not responsible for the conduction of free electrons and so the electrons complete the half reaction will move through an extra external wire. In discharging, the lithium ions are extracted from the anode and move back to the cathode.

Graphite is currently the most common material used for the anodes of commercial batteries because of its capability for reversible lithium intercalation in the layered crystals (which represents the theoretical lithium storage capacity, around, 372 mAh/g as LiC_6) [2]. Although attempts have been made to find suitable replacements, currently only carbonaceous materials (natural graphite, carbon fiber and metal deposited carbon fiber) are used in commercial anodes and there are no theoretical or experimental reports from graphene doped anode cell interaction in LIBs. The favorable electrochemical efficiency of LIBs regarding energy and power densities, as well as the progress in manufacturing and cell design, have made LIBs greatly successful for devices electronics. LIBs basically consists of a positive electrode, a negative electrode and a conducting electrolyte where store electrical energy in the two electrodes in the form of Li-intercalation compounds. Electrolyte, electrodes and separator are the main components of the LIB where the anode plays an essential role in the efficiency of these devices.

Numerous experiments have been performed to confirm the application of graphene nano-sheets to increase lithium storage capacity and to improve recharge cyclic efficiency [3-6]. There are a number of reviews on anode materials [4-12] and many of them focus on both carbon and inorganic materials. Furthermore semi-empirical and first-principal calculations have been used to investigate lithium ion storage states between two graphene sheets [6], as well as some heteroatom-substituted carbon materials [7]. Discharging and charging of Li-ions in graphitized carbon is well established up to now [12–17].

Scaling down the particle size, while effective for improving diffusivity in cathode materials, may not be an option in carbonaceous anode materials, as the increased surface area leads to higher lithium consumption during SEI formation. Most reports on Li-ion diffusivity address improving measurement techniques and not the diffusion mechanism itself. This may derive from the various phase mixtures, the staging phenomenon of graphite, and the complexity caused by the SEI film

This work has investigated to find the suitable concentration of Li+/Li in replacement for carbonaceous materials and illustrate a novel mechanism of the graphite-anode cell interaction Scheme.1. As the efficiency of LIB including cycle life, power density and energy density is strongly influenced by anode materials, some of the certain characteristics to maximize the battery performance have been considered in our model. These items are including fast diffusivity of lithium ion, critical changes in the crystal structure of anode material (during intercalation-de-intercalation by Li ions), required low potential of anode materials to supply a high cell voltage with the cathode and capability of storing a significant amount of charge (coulomb) per unit mass is necessary.

Conduction in anode's material is complex due to continuous phase transformations and the formation of the solid–electrolyte interphase (SEI) layer [18, 19]. In this work, to clarify the mechanisms related to the properties and performance of Li-ion batteries, the exact investigation of the electronic state and the diffusion process in the carbon and the SEI layer is still required. The SEI layer displays much lower electronic and ionic conductivity compared to the bulk electrode. The diffusion process

can vary widely from carbonaceous materials to non-graphitic materials [20-22]. Boron doped graphite has also been researched as an option to enhance electrochemical efficiency [23-29]. Using the surfaces of graphene electrodes including h-BN dielectric in anode materials, boron nitride doped graphite, and other kinds of X-doped graphene (X=Be, Li) has been shown to increase cell performance by this work scheme 1.

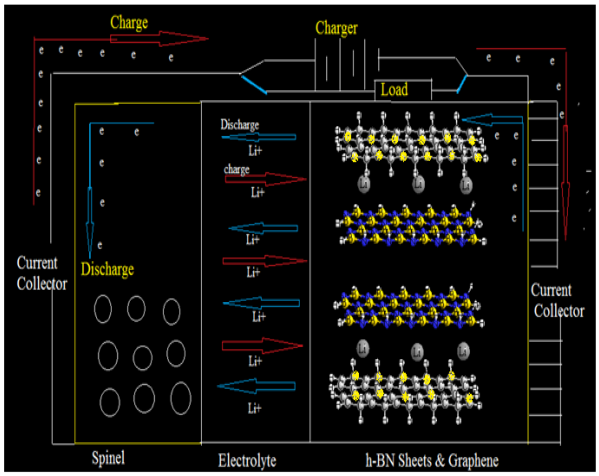

Scheme.1. Operating Li-ion battery.

The bonding orbit π of B-N is generally dominated via 2*p* orbitals of N, while 2*p* orbitals of B contribute basically to the anti-bonding orbital of π∗. This indicates a considerable charge transfer from B to N, around 0.42 electrons. In contrast, there is no important electron transfer in the C-C bonding, therefore the B-N bonding is essentially ionic; while C-C bonding is covalent (This also leads to the different electron band structure).

The sp^2-hybridization related to B-N and C-C bonds have very similar behavior in mechanics, while the large differences in optics and electronics.

1.1. Li^+ diffusivity

Electronic properties of graphite and h-BN are radically different from each other. It has been shown theoretically the calculations for the band structure of the graphite mono layer and h-BN [31, 32]. For a graphene layer, two bands cross each other at the Fermi energies. So, graphene has a semimetal behaviour. In contrast of graphene, for h-BN mono layer, similar bands do not cross each other, therefore a 4.55 eV band gap forms in this position. Experimentally, bulk h-BNs have been measured to have a band gap of 5.85 eV [33-35]. H-BN Multilayers has a wide band gap insulator which might vail as a dielectric material among metal-doped graphene layers. Moreover, the plates which are lattice matched to graphene allow one to attain sturdy and high accuracy nanoscale spacing among a few paralleled metallic graphene plates, which can be set to favorable values.

These graphene -based materials consist of few-layer-stacked h-BN nano-crystallites with large interlayer distances in the range of 0.333–0.335 nm in the graphene/h-BN/graphene as anode. Both experimental and theoretical approaches of metallic properties for graphene were investigated on understanding the dielectric behavior of these structures to form thin layers which can bestead as charging holder plates [34, 35 and 36]. Furthermore they were exhibited that graphene can preserve current densities six orders of magnitude larger than copper. In graphite, the stacking is slightly different; hexagons are offset and do not lie on top of each other. Interlayer distances are similar: 3.35 Å for graphite [30] and 3.33 Å for h-BN. An ideal form of an anode material should be composed of metal-doped on graphene layers including a dielectric material between these layers for increasing the capacitance value that can store and release charge quickly. It has been theoretically [30-39] and experimentally shown that h-BN layers of any thickness can be grown on graphene layers and it is also possible to flourish perpendicular carbon on top of the sheets [41-43]. In this study, charging and discharging of Li-ions has investigated in h-BN with the positive electrode reaction as: $LiCoO2 \rightleftarrows Li\ (1-x)\ CoO2 + x\ Li+ + x\ \bar{e}$ and the negative electrode reaction as: $xB_3N_3 + x\ Li^+ + x\bar{e} \rightleftarrows x\ Li\ B_3N_3$, while the whole reaction is: $LiCoO2 + x\ B_3N_3 \rightleftarrows Li_{1-x}CoO2 + x\ Li\ B_3N_3$ **(1)**. It has been suggested that lithium atoms are stored via two mechanisms: intercalation and alloying. Electrical conductivity (Scm^{-1}) of graphite, Li-GIC under various conditions are 1.89×10^4 for graphite (parallel direction with respect to graphene layer), 2.45×10^5 for Li-GIC, 2.5×10^2, for graphite thin film (bulk graphite), and 3.0×10^1 for ten-layers of thin films. The energy stored is liberated when the plates are connected to a circuit, so that the discharged electrodes shift into an equilibrium state. So the Li^+ insertion in $(BG//(h\text{-}BN)_n//BG)$ occurs in a large capacity (mAh/g) from Concentration of Li/Li+ towards the efficiency of Lithium ion batteries. Although the materials used as electrodes for Li storage should have binding strength with Li within a certain range, binding to anode material matrix (M) should be weaker than on the cathode side. The matrix binding energy "E_{Li-M}", can be determined from the curves asE_{Li-M}, $-E_{Li} = -\frac{E_x}{x}$ **(2)** (It is linearly related to the average discharge voltage). In Li-ion batteries, the Li+ ions arrive at the surface and are adsorbed on matrix in eq.3 . μ(Li@ Li_x M = [E (Li_x M –E (M)]/X-TS **(3).** Based on the determined most stable structures, we estimate the formation energy of system. The formation free energy ΔG (m) of each cluster at concentration x is defined as: ΔG (m) = E (Li_m@M-E (M)-m μ(Li@ Li_x M) **(4)**. where μ(Li@ Li_x M is the chemical potential of Li under various conditions. The entropy of the reference phase is estimated by counting the number of adsorption configuration at a given concentration. The entropy S (per adsorbed Li atom) of the adsorbed phase is given by: -S(x) $= -S(x) = K_B[ln2x + \frac{(1-2x)\ln(1-2x)}{2x}]$ **(4),** where x is the Li: C ratios ranging and K_B is the Boltzmann constant. The lithiation depends strongly on the chemical potential of Li atoms. The cluster energy would be negative, and the formation of Li clusters is strongly favored, if the chemical potential is chosen to be that of atomic Li. whereas the formation energy is positive (meaning that cluster formation is unlikely), if the chemical potential is chosen to be that of Li in the bulk phase. We also include the configurationally entropy correction at an attenuate limit into the chemical potential of the reference phase. The interaction between anode matrix and Li clusters is stronger than that of neutral metallic bulk Li on matrix, which indicates the stronger ionic bonding and charge transfer from Li to anode material. The Li electrons should be localized inside the cluster during the formation of cluster, similar to bulk Li where each Li has zero net charges. At intermediate cluster sizes, the transition from the Li to bulk behavior occurs.

In this work several lithium have applied as insertion function for investigating of our model (scheme 2). In the cluster by two atoms "Li_2" in vacuum, the Li electrons pair up and form the Li-Li bond. However, when adsorbed on boron doped graphene, our calculations indicate that the Li electrons are mainly transferred to graphene by filling up the upper Dirac cone, as shown in. It can be suggested that the Li_2 is ionized and each Li carries +1 charge.

For Li3, a flat band appears below the Fermi level. Its charge density distribution indicates that two electrons are shared between the Li3 clusters. The remaining electron is transferred to graphene. Therefore, on average, each Li carries +1/3 charge. Diffusion properties of Li-ion cell determine some of the key performance metrics of Li-ion battery cells, including the charge and discharge rate, practical capacity and cycling stability. The governing equation describing the diffusion process is known as Fick's law as:

$j_i = -D_i \nabla C_i$ **(1)** And $\frac{\sigma C_i}{\sigma t} = \nabla.(D \nabla C_i)$ **(2)** where "j_i" is ionic flux, molcm^{-2} s^{-1}, D_i is diffusivity of solute (i =1, 2), cm^2 s^{-1} and C_i is concentration of species "i", (molcm3) [60]. The proportionality factor D is the diffusivity or diffusion coefficient as $D_i = \frac{K_B T}{6\pi\mu R_0}$ **(4)** .

For Li_n (n=even) two electrons are localized inside the cluster, and thus each Li has +1/2 charge averagely. The adsorption and mechanism of electron density in anode matrix for LiB3C3 is shown in, the Li_2 atom to bulk LiB3C3 of large size. All the numbers are positive, indicating that the compound is indeed stable. Although in the Li loses its 2*s* electron to C, producing ionic Li–C bonding, the bonding energies are different: $E_{Li-boron\ doped\ graphene} > E_{Li} > E_{Li-graphene}$. Therefore, when loaded with Li, the energy of Li–boron doped graphene system drops due to the increase in the favorable Li–boron doped graphene bonding, until reaching the LiB_nC_m composition, where further Li loading 5 results in a strong repulsion between Li-ions at neighboring hexagons.

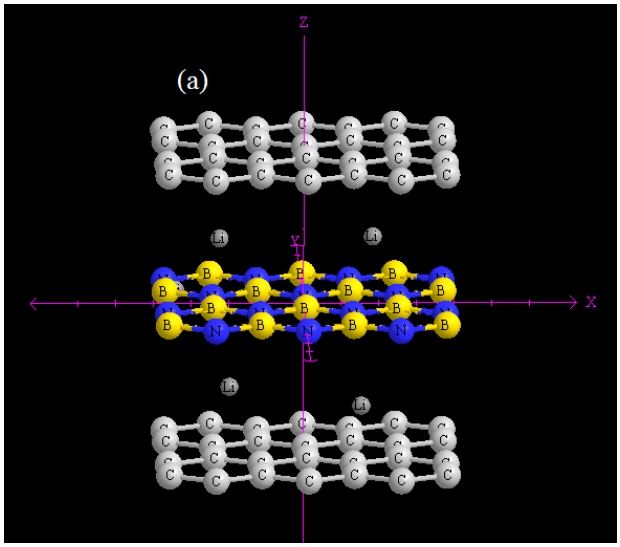

Scheme 2. Li diffusion.

In condensed materials both liquids and solids, diffusion is governed by random jumps of atoms or ions, leading to position exchange with their neighbors. The kinetics of this process is temperature dependent and follows an Arrhenius type relationship $rate \approx \exp\left(-\frac{\Delta G}{k_B T}\right)$**(5)** . In liquids, the temperature dependence of the diffusion is much less than in solids. Note that no successful first-principles calculation has been made, due to insufficient understanding of the liquid structure. Thus, a simple expression derived from Stoke's drag law is frequently used
as an alternative for a diffusivity expression in liquids (Eq. 3).

Thus diffusion can be the rate-determining process compared to electronic conduction in an electrochemical reaction. The van der Waals interaction, expressed as the Lennard–Jones potential, is relatively weak despite showing a longer interaction range. In the case of the graphite anode, a Li-ion can easily diffuse parallel rather than perpendicular to the graphene layers during intercalation. Thus in order to understand the diffusion of the Li-ion it is important to consider crystal structure as well as the surrounding potential

1.2. Densities energy in diffusion

The electron densities have been defined as $\rho(r) = \eta_i \left|\varphi_i(r)\right|^2 = \sum_i \eta_i \left|\sum_l C_{l,i}\, \chi_i(r)\right|^2$ **(6).** Where η_i indicates an occupation number of related orbitals (*i*), φ is l wave function, χ is basis set function and C is the coefficient matrixes, of orbital j respect to basis function i. Atomic unit for electron density can be explicitly written as e/Bohr^3. $\nabla\rho(r) = [(\frac{\partial\rho(r)}{\partial(x)})^2 + (\frac{\partial\rho(r)}{\partial(y)})^2 + (\frac{\partial\rho(r)}{\partial(z)})^2]^{\frac{1}{2}}$ **(7)** $\nabla^2\rho(r) = \frac{\partial^2\rho(r)}{\partial x^2} + \frac{\partial^2\rho(r)}{\partial y^2} + \frac{\partial^2\rho(r)}{\partial z^2}$**(8)**.

The positive and mines data of these functions correspond to the electron densities are locally depleted and locally concentrated respectively. The relationships between $\nabla^2\rho$ and valence shell electron pair repulsion (VSEPR) model, chemical bond type, electron localization and chemical reactivity have been built by Bader [68]. We have calculated the Density and energy of lithium in diffusion model for 6 lithiom inside the C_x-BN electrods of C_x-BN// $(h\text{-}BN)_n$//C_x-BN LIBTs (the carbon fractions are %14, %18 and %27 for the three representative nano-sheets denoted as $C_{0.3}$-BN, $C_{0.4}$-BN and $C_{0.7}$-BN, respectively).
The kinetic energy density is not uniquely defined, since the expected value of kinetic energy operator
$< \varphi\ |-\left(\frac{1}{2}\right)\nabla^2|\ \varphi >$ can be recovered by integrating kinetic energy density from alternative definitions. One of the commonly used definition is: $k(r) = -\frac{1}{2}\sum_i \eta_i \varphi_i^*(r)\nabla^2\varphi_i(r)$ **(9)** Relative to K(**r**)(66), local kinetic energies given as follow guarantee positivizes; hence its physical meaning is more commonly used. The Lagrangian kinetic energy density, "G(r)" is also known as positive definite kinetic energies densities.
$G(r) = \frac{1}{2}\sum_i \eta_i \left|\nabla(\varphi_i\right|^2 = \frac{1}{2}\sum_i \eta_i\{[(\frac{\partial\varphi_i(r)}{\partial(x)})^2 + (\frac{\partial\varphi_i(r)}{\partial(y)})^2 + (\frac{\partial\varphi_i(r)}{\partial(z)})^2]\}$
(10). K(**r**) and G(**r**) are directly depended to Laplacian's electron density $\frac{1}{4}\nabla^2\rho(r) = G(r) - K(r)$ (65-67)**(11)**
Becke and Edgecombe noted that spherically averaged likespin conditional pair probability has direct correlation with the Fermi hole and then suggested electron localization function (ELF) .ELF(r) $= \frac{1}{1+[D(r)/D_{0(r)}]^2}$ **(12)** where D(r) $= \frac{1}{2}\sum_i \eta_i \left|\nabla\varphi_i\right|^2 - \frac{1}{8}[\frac{\left|\nabla\rho_\alpha\right|^2}{\rho_\alpha(r)} + \frac{\left|\nabla\rho_\beta\right|^2}{\beta(r)}]$ **(13)** and $D_{0(r)} = \frac{3}{10}(6\pi^2)^{\frac{2}{3}}[\rho_\alpha(r)^{\frac{5}{3}} + \rho_\beta(r)^{\frac{5}{3}}]$ **(14)** for close-shell system, since $\rho_\alpha(r) = \rho_\beta(r) = \frac{1}{2}\rho$

, D and $D0$ terms can be simplified as $D(r) = \frac{1}{2}\sum_i \eta_i \ |\nabla\varphi_i|^2 - \frac{1}{8}[\frac{|\nabla\rho|^2}{\rho(r)}]$ **(15)**, $D_{0(r)} = \frac{3}{10}(3\pi^2)^{\frac{2}{3}}\rho(r)^{\frac{5}{3}}$ **(16).**

Savin *et al*. have explained ELF in viewpoint of kinetic energies, which causes ELF meaningful for Kohn-Sham DFT wave-functions. They indicated that $D(\mathbf{r})$ reveals the excess kinetic energies densities caused by Pauli repulsion, while $D0(\mathbf{r})$ can be considered as Thomas-Fermi kinetic energies densities.

Localized orbital locator (LOL) is another function for locating high localization regions likewise ELF, defined by Schmider and Becke in the paper.

Local information entropy is a quantification of information, this theory was proposed by Shannon in his study of information transmission in noise channel, and nowadays its applications have been tightly widened to other areas, including theoretical approaches. As instance, Aslangul and coworkers tried to decompose diatomic and triatomic molecules into mutually exclusive spaces through interpretation information entropies.

Parr *et al.* discussed the relationship between information entropy and atom partition as well as molecular similarity .Noorizadeh and Shakerzadeh suggested using information entropy to study aromaticity . The formula of Shannon's information entropy for normalized and continuous probability function is $S = -\int P(x)\ln P(x)dx$ **(19)**. For chemical system, if $P(x)$ is replaced by$\frac{\rho(r)}{N}$, then the integrand may be called local information entropy of electrons. $S(r) = -\frac{\rho(r)}{N}\ln\frac{\rho(r)}{N}$ **(20)** Where, N is the total number of electrons in current system.

$LOL(r) = \frac{\tau(r)}{1+\tau(r)}$ **(17)**, where $(r) = \frac{D_0(r)}{\frac{1}{2}\sum_i \eta_i \ |\nabla\varphi_i|^2}$ **(18)**, $D_0(r)$ for spin-polarized system and close-shell system are defined in the same way as in ELF [73]. We have calculated the Hamiltonian kinetic energy and density Electron localization function of lithium in diffusion model for 6 lithium inside the C_x-BN electrods of C_x-BN// (h-BN)$_n$//C_x-BN LIBTs (the carbon fractions are %14, %18 and %27 for the three representative nano-sheets denoted as $C_{0.3}$-BN, $C_{0.4}$-BN and $C_{0.7}$-BN, respectively).

Table 1. The diffused lithium (N=1 to N=5)

1 Li Charge		2 Li Charge		3 Li Charge		4 Li Charge		5 Li Charge	
Mulliken	ESP fit	Mullikan	ESP fit	Mullikan	ESP fit	Mullikan	ESP fit	Mullikan	ESP fit
-0.234	0.0486	-0.094	0.0299	-0.142	0.0597	-0.142	0.0606	0.2210	0.0846
-0.081	-0.000	-0.194	0.0055	0.3337	0.0146	0.3337	0.0188	0.5006	0.0343
0.0002	-0.007	-0.155	0.0034	-0.155	0.0085	-0.265	0.0202	-0.265	0.0199
0.0002	0.0065	-0.122	0.0344	-0.122	0.0332	-0.191	0.0708	-0.191	0.0706

The ESP evaluated under default value is accurate enough in general cases. Reduced density gradient (RDG) RDG and *Sign* $(\lambda 2)*\rho$ are a pair of very important functions for revealing weak interaction region, [135] for detail. The basic applications are exemplified in Sections 4.100.1 and 4.200.1. RDG is defined as $RDG(r) = \frac{1}{2(3\pi^2)^{\frac{1}{3}}}\frac{|\nabla\rho(r)|}{\rho(r)^{\frac{4}{3}}}$ **(21)** by default x is 0.05; it can be nullify this treatment by setting the parameter to zero.

There are a lot of reviews on ESP, interested readers are suggested to consult.

$\rho^{pro}(r) = \sum_A \rho_A^{free,fit}(r - R_A)$ Where $\rho_A^{free,fit}$ **(22)** is pre-fitted spherically averaged electron density of atom a . We have calculated the local information entropy and electrostatic potential of lithiums in diffusion model for the "C_x-BN" electrods of the "C_x-BN// (h-BN)$_n$//C_x-BN" LIBTs. (The carbon fractions are 14, 18 and 27 at. % for the three representative nano-sheets denoted as $C_{0.3}$-BN, $C_{0.4}$-BN and $C_{0.7}$-BN, respectively. The representative atomic charges for molecules should be computed as average values over several molecular conformations [30-35].

2. MATERIALS AND METHODS

Calculations were performed using GAMESS-US packages. In this study, we have particularly concentered on getting the optimized data for each tube from DFT calculation including the m06 and m06-L. Pm6, Extended-Huckel and Pm3MM including pseudo=lanl2 calculations using Gaussian program have done for the non-bonded interaction between two tubs. We employed density functional theory with the van der Waals density functional to model the exchange-correlation energies of h-BN sheets. The double ζ-basis set with polarization orbitals (DZP) were used for x lithium over the h-BN sheets.

The B3LYP and most other functional are correctly insufficient to illustrate the exchange and correlation energy for distant non-bonded medium-range systems. Moreover, some recent studies have shown that inaccuracy for the medium-range exchange energies leads to large systematic errors in the prediction of molecular properties [36- 39].

We further calculated the interaction energy between x lithium h-BN sheets. The interaction energy was calculated via an Mp6 method in all items according to eq.23:

$\Delta E_S(eV) = \{E_{total} - (E_{xLi} + E_{h-BNsheets})\} + E_{BSSE}$ **(23)** Where the "ΔE_S" is the stability energy of system. The electron density (Both of Gradient norm & Laplacian)have been calculated, value of orbital wave-function, electron spin density, electrostatic potential from nuclear/atomic charges, electron localization function (ELF), localized orbital locator (LOL defined by Becke & Tsirelson), total electrostatic potential (ESP) and the exchange-correlation density, correlation hole and correlation factor, Average local ionization energy using Multifunctional Wave-function analyzer .

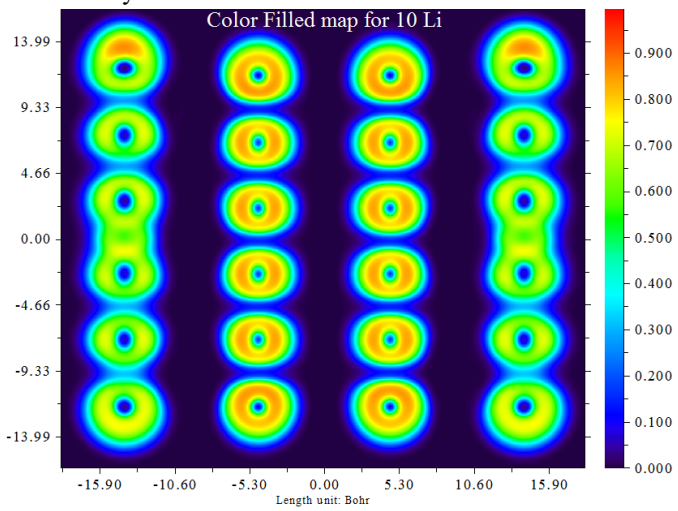

Figure 1. Densities of lithium between h-BN and graphene.

In such a condition, variations of the innermost atomic charges will not lead towards a significant change of the MESP outside of the molecule, meaning that the accurate values for the innermost atomic charges are not well-determined by MESP outside the molecule. This approach (CHELPG) is shown to be considerably less dependent upon molecular orientation than the original CHELP program. The results are compared to those obtained by using CHELP.

Some of our previous work has been applied for improving our calculations [40-74]. The contour line map has drawn via Multiwfn software [75]. The relief map has used to present the height value at every point. If values are too large they will be truncated in the graph, it can be chosen to scale the data with a factor to avoid truncation. The graph is shown on interactive interface. Shaded surface map and shaded surface map with projection are used in our representation of height value at each situation.

3. RESULTS

We have listed the data of density, energy, electron localization function (ELF), localized orbital locator (LOL) and local entropy, gap energy, charge from ESP, electrostatic potential, ionization energy, the charges of two BN-graphene electrodes and the stability energy of several lithium insertion (concentration of Li+)(tables1,2) and these data have plotted in the figures (Figs.1-8).

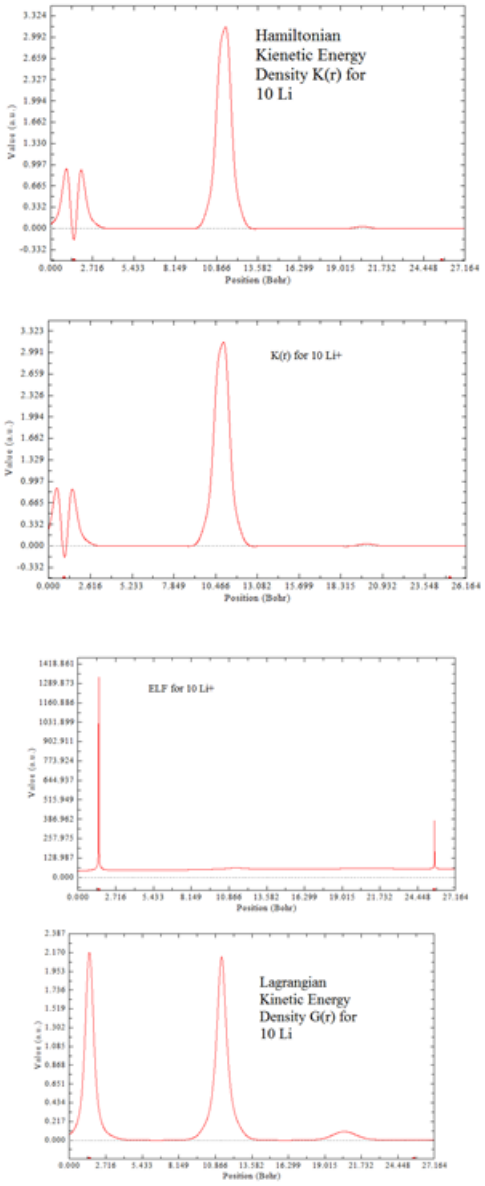

Figure 2. ELF and LOL of 10 cluster lithium with optimized dimension between two layers of h-BN and two electrodes of B doped graphene.

We have calculated the gradient norm and the Laplacian of electron density via Eqs **(7, 8)** for the lithium diffused in the batteries system respectively and the data are listed in table1-2. For calculation the electron spin density from the difference between alpha and beta density, we have Used $\rho^s(r) = \rho^\alpha(r) - \rho^\beta(r)$ then the spin polarization parameter function will be returned instead of spin density $\xi(r)=\frac{\rho^\alpha(r)-\rho^\beta(r)}{\rho^\alpha(r)+\rho^\beta(r)}$ .The data of ξ going from zero to unity corresponds to the local area going from un-polarized case to completely polarized case Table1.

The kinetic energies densities, Lagrangian, and the electrostatic potential can be calculated as eqs. (9), (10) and: $V_{nuc}(r) = \sum_A \frac{Z_A}{|r-R_A|}$ where RA and ZA denote position vector and nuclear charge of atom A, respectively and are listed in tables1, 2.

If electrons are completely localized, then they can be distinguished from the ones outside. In which kinetic term in $D(\mathbf{r})$ from eqs. 15-16 is replaced by Kirzhnits second-order expansion, that is $\frac{1}{2}\sum_i \eta_i \ |\nabla\varphi_i|^{\ 2} \approx D_0(r) + \frac{1}{72}\frac{|\nabla\rho|^{\ 2}}{\rho(r)+\frac{1}{6}\nabla^2\rho(r)}$ so that ELF is totally independent of wave-function, and then can be used to analyze electron density from X-ray diffraction data.

Bader explained that the large electron localization have a large amount of Fermi hole. ELF is within the range of [0, 1]. A large ELF means which electrons are largly localized, due to a covalent bond. LOLs datahave same expression compared to ELF. Actually, LOL and ELF are generally qualitative comparable, while Jacobsen pointed out that LOL conveys more decisive and obvious picture than ELF, So LOL can be interpreted in kinetic energy way as for ELF. Small or large LOL data usually appears in boundary or inner region of localized orbitals. The value range of LOL is identical to ELF, namely [0, 1].

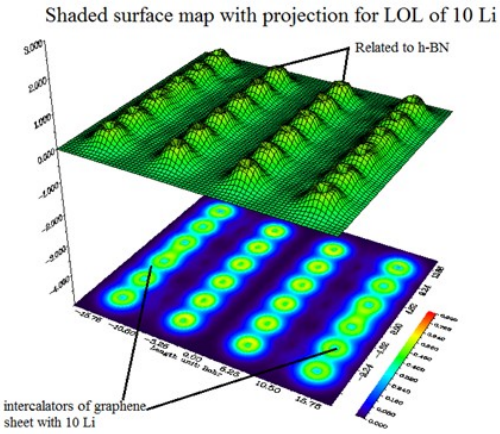

Figure 3.electron density of B-graphene//(h-BN)$_2$//B-graphene indicates a negative plate and positive plate of B3C3 electrodes.

As lithium has an unpaired electron, leading to a difference in spin-up and spin-down, when two lithium atoms are adsorbed simultaneously electrons get paired and magnet moment disappears.

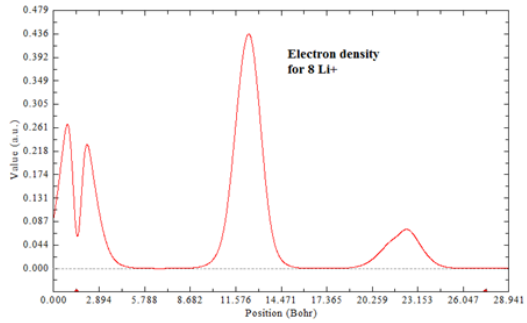

Figure 4. Electron densities for all atoms in Li_8-B_3C_3 complexes.

As a result, spin polarized cluster has a gap which size depends on adsorbed electron spin polarization.

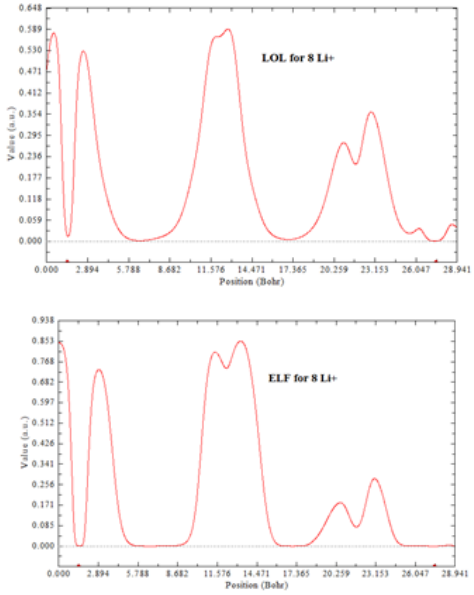

Figure 5. LOL and ELF for the electron localization (ELF) for all atoms in Li_8-B_3C_3 complexes.

In this work we have calculated the local Information entropy for each lithium atom via eqs. 19-20 and the integrating of this function over whole space yields the information entropy. The data of local Information entropy are listed in Tables 1-3. Weak interaction (eqs 20-21) has a significant influence on conformation of macromolecules,; however reproduction of electron density by *ab initio* and grid data calculation of reduced density gradient (RDG) for such huge systems are always too time-consuming.

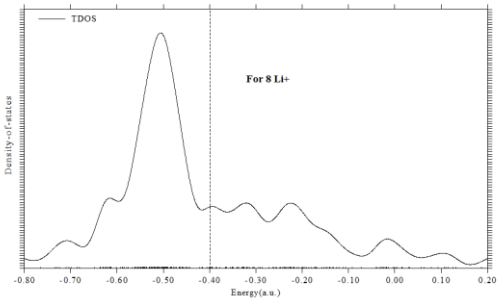

Figure 6. DOS for 10 Li/Li+ simulation of LIBTs.

By this work, we have shown the Concentration of Li/Li+ towards the efficiency of Lithium ion batteries which demonstrate high electrical conductivity, good mechanical strength, excellent flexibility, great chemical stability and high specific surface area. This is especially noticeable when graphene is chemically converted with a greater proportion of functional groups, proving that it is suited for use as a base composite electrode material.

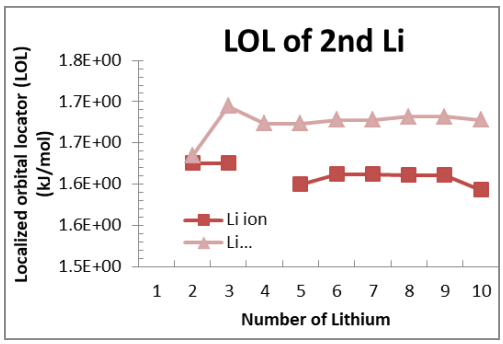

Figure 7. LOL versus concentration of Lithium numbers.

When used as electrode material, G-(h-BN)$_2$-G can effectively reduce the size of the active material, prevent agglomeration of nanoparticles, improve electrons and ions transmission capacity, as well as enhancing the electrode's mechanical stability.

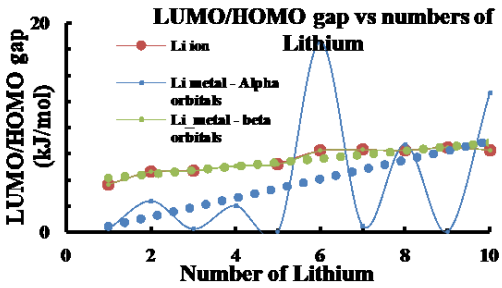

Figure 8. The LUMO and HOMO gap versus Li+/Li concentration.

As a result, G-(h-BN)$_2$-G -containing electrode materials have high capacity and good rate performance. G-(h-BN)$_2$-G flexibility makes it an ideal material to buffer metal electrode's volume expansion and contraction during the charge– discharge process. Further, the excellent electrical properties of G-(h-BN)$_2$-G can enhance the conductivity of metal electrode material. Smaller particles mean the diffusion distance of lithium ions and electrons is reduced, this improves the material's rate performance. Finally, the lithium storage capacity for most metal oxide composite materials with G-(h-BN)$_2$-G can be useful greatly.

Table 2. The layers distance and ESP compare to Mullikan charges.

layer Distance			1 Li
(Å)	(m)	Name	Mulliken
5.015	5.015E-10	1-2 (G-BN)	-0.15331
4.94	4.940E-10	2-4 (BN-BN)	-0.081232
5.015	5.015E-10	4-3 (BN-G)	0.000418
14.97	1.497E-09	**1-3 (4 sheets)**	**-0.31538**
		å Li charge	1.315382
		å system	1.000002
2 Li	2 Li	3 Li	3 Li
Mulliken	ESP fit	Mulliken	ESP fit
0.099844	0.02439	0.191519	0.045112
-0.071721	-0.028893	-0.211006	-0.018658
0.032465	0.030978	0.032508	0.024675
-0.566943	**0.07343**	**-0.753881**	**0.116217**
2.566946	1.926572	3.75388	2.883789
2.000003	2.000002	2.999999	3.000006

4. CONCLUSIONS

In contrast to graphite, BN layers is transparent and is an insulator. In BN layers boron atoms in one layer are located directly on top of nitrogen atoms in neighboring layers and vice versa and the hexagons lie on top of each other. In our previous works [28,29]we have reported a nanoscale dielectric Li batteries to consist of two metallic graphene layers separated by insulating h-BN thin layers that have been successfully used to simulate structures of graphene/h-BN/graphene.

5. REFERENCES

1. Cheng, F.; Liang, J.; Tao, Z.; Chen, J. Functional materials for rechargeable batteries. *Advanced Materials* **2011,** *23*, 1695-1715, https://doi.org/10.1002/adma.201003587.
2. Whittingham, M.S.; Materials challenges facing electricalenergy storage. *MRS Bulletin* **2008,** *33*, 411-419, https://doi.org/10.1557/mrs2008.82.
3. She-huang, W.; Su, H.S. Electrochemical characteristics ofpartially cobalt-substituted LiMn2-*y*Co*y*O4 spinels synthesizedby Pechini process. *Materials Chemistry and Physics* **2002**, *78,* 189–195, https://doi.org/10.1016/S0254-0584(02)00346-2.
4. Tarascon, J.M.; Armand, M. Issues and challenges facingrechargeable lithium batteries. *Nature* **2001,** *414*, 359-367, https://doi.org/10.1038/35104644.
5. Nagaura, T.T.K. Lithium ion recheargable battery. *Progress in Batteries & Solar Cells***. 1990,** *9*, 209.
6. Scrosati, B.; Garche, J. Lithium batteries: Status, prospects and future. *Journal of Power Sources* **2010,** *195*, 2419-2430, https://doi.org/10.1016/j.jpowsour.2009.11.048.
7. Whittingham, M.S. Lithium Batteries and Cathode Materials. *Chemical Reviews* **2004**, *104*, 4271-4302, https://doi.org/10.1021/cr020731c.
8. Bruce, P.G.; Scrosati, B.; Tarascon, J.M. Nanomaterials for Rechargeable Lithium Batteries. *Angewandte Chemie International Edition* **2008,** *47,* 2930-2946, https://doi.org/10.1002/anie.200702505.
9. Goodenough, J.B.; Kim, Y. Challenges for Rechargeable Li Batteries. *Chemistry of Materials* **2009,** *22*, 587-603, https://doi.org/10.1021/cm901452z.
10. Kaskhedikar, N.A.; Maier, J. Lithium storage in carbon nanostructures. *Advanced Materials* **2009,** *21*, 2664-2680, https://doi.org/10.1002/adma.200901079.
11. Cabana, J.; Monconduit, L.; Larcher, D.; Palacin, M.R. Beyond intercalation-based Liion batteries: The state of the art and challenges of electrode materials reacting through conversion reactions. *Advanced Materials* **2010,** *22*, 170-192, https://doi.org/10.1002/adma.201000717.
12. Poizot, P.; Laruelle, S.; Grugeon, S.; Dupont, L.; Tarascon, J.M. Nano-sized transition-metaloxides as negative-electrode materials for lithium-ion batteries. *Nature* **2000,** *407*, 496-499, https://doi.org/10.1038/35035045.
13. Park, J.C.; Kim, J.; Kwon, H.; Song, H. Gram-Scale Synthesis of Cu2O Nanocubes and Subsequent Oxidation to CuO Hollow Nanostructures for Lithium-Ion Battery Anode Materials. *Advanced Materials* **2009,** *21*, 803, https://doi.org/10.1002/adma.200800596.
14. Ban, C.M., Wu, Z.C.; Gillaspie, D.T.; Chen, L.; Yan, Y.F.; Blackburn, J.L.; Dillon, A.C. Nanostructured Fe3O4/SWNT Electrode: Binder-Free and High-Rate Li-Ion Anode. *Advanced Materials* **2010,** *22*, 145, https://doi.org/10.1002/adma.200904285.
15. Doh, C.H.; Kalaiselvi, N.; Park, C.W.; Jin, B.S.; Moon, S.I.; Yun, M.S. Synthesis and electrochemical characterization of novel high capacity Si3-xFexN4 anode for rechargeable lithium batteries. *Electrochemistry Communications* **2004,** *6*, 965-968, https://doi.org/10.1016/j.elecom.2004.07.011.
16. Cabana, J.; Stoeva, Z.; Titman, J.J.; Gregory, D.H.; Palacin, M.R. Towards new negative electrode materials for Li-ion batteries: Electrochemical properties of Li-Ni-N. *Chemistry of Materials* **2008,** *20,* https://doi.org/10.1021/cm7034486.
17. Morgan, D.; Van der Ven, A.; Ceder, G. Li conductivity in LixMPO4 (M = Mn, Fe, Co, Ni) olivine materials. *Electrochemical and Solid State Letters* **2004,** *7*, 30-32, https://doi.org/10.1149/1.1633511.
18. Muraliganth, T.; Murugan, A.V.;Manthiram, A. Nano scale networking of LiFePO4 nano rods synthesized by a microwavesolvo thermal route with carbon nanotubes for lithium ion batteries. *Journal of Materials Chemistry* **2008,** *18*, 5661-5668, http://dx.doi.org/10.1039/b812165f.
19. Yamada, A.; Chung, S.C.; Hinokuma, K. Optimized LiFePO4 for lithium battery cathodes. *Journal of the Electrochemical Society* **2001,** *148*, 224-229, https://doi.org/10.1149/1.1348257.
20. Wang, Y.G.; Wang, Y.R.; Hosono, E.J.; Wang, K X.; Zhou, H.S. The design of a LiFePO4/carbon nano-composite with a core-shell structure and its synthesis by an in situ polymerization restriction method. *Angewandte Chemie-International Edition* **2008,** *47*, 7461-7465, https://doi.org/10.1002/anie.200802539**.**
21. Zhou, Y.; Wang, J.; Hu, Y.; O'Hayre, R.; Shao, Z. A porous LiFePO4 and carbon nanotube composite. *Chemical Communications* **2010,** *46*, 7151-7153, https://doi.org/10.1039/C0CC01721C.
22. Liu, J.; Conry, T.E.; Song, X.; Doeff , M.M.; Richardson, T.J. Nano-porous spherical LiFePO4 for high performance cathodes. *Energy & Environmental Science* **2011,** *4,* 885-888, https://doi.org/10.1039/c0ee00662a.
23. Saravanan, K.; Balaya, P.; Reddy, M.V.; Chowdari, B.V.R.; Vittal, J.J. Morphology controlled synthesis of LiFePO4/C nano plates for Li-ion batteries. *Energy & Environmental Science* **2010,** *3,* 457-464**,** https://doi.org/10.1039/B923576K.
24. Srinivasan, V.; Newman, J. Discharge model for the lithium iron-phosphate electrode. *Journal of the Electrochemical Society* **2004,** *151*, 1517-1529, https://doi.org/10.1149/1.1785012.
25. Akimoto, J.; Gotoh, Y.; Oosawa, Y. Synthesis and Structure Refinement of LiCoO2 Single Crystals. *Journal of Solid State Chemistry* **1998**, *141*, 298-302.
26. Madhu, C.; Garrett, J.; Manivannan, V. Synthesis and characterization of oxide cathode materials of the system (1-y)LiNiOxLiMnOyLiC oO. *Ionics* **2010**, *16*, 591-602.
27. Sun, Y. The preparation and electrochemical performance of solid solutions LiCoO2–Li2MnO3 as cathode materials for lithium ion batteries. *Journal of Power Sources* **2006**, *159*, 1353-1359, https://doi.org/10.1016/j.jpowsour.2005.12.037.
28. Jiang, J. Structure, Electrochemical Properties, and Thermal Stability Studies of Cathode Materials in the xLi [Mn 1/2] NiOy LiCoOzLi [Li1/3] Mn[2/3] O2 Pseudoternary System (x + y + z = 1). *Journal of The Electrochemical Society* **2005**, *152*, 1879-1889.
29. Zhong, Q. Synthesis and Electrochemistry of LiNiMn- xO2 *Journal of the Electro -chemical Society*. **1997**, *144,* 205-213.
30. Zhong, S.W.; Zhao, Y.J.; Li, Y.; Li, P.Z.; Mei, J.; Liu, Q.G. Characteristics and electrochemical performance of cathode material Co coated LiNiO2 for Li-ion batteries. *Transactions of Nonferrous Metals Society of China* **2006**, *16*, 137-141,

https://doi.org/10.1016/S1003-6326(06)60024-1.
31. Amatucci, G.; Pasquier, A.D.; Blyr, A.; Zheng, T.; Tarascon, J.M. The elevated temperature performance of the LiMn2O4/C system: failure and solutions. *Electrochimica Acta* **1999,** *45*, 255-271, https://doi.org/10.1016/S0013-4686(99)00209-1.
32. Liu, L.; Wang, Z.; Li, H.; Chen, L.; Huang, X. Al2O3-coated LiCoO2 as cathode material for lithium ion batteries. *Solid State Ionics* **2002**, *152*, 341, https://doi.org/10.1016/S0167-2738(02)00333-8.
33. Mikhaylik, Y.V.; Akridge, J.R. Low Temperature Performance of Li/S Batteries. *J. Electrochem. Soc.* **2003,** *150*, 306.
34. Colfen, H.; Mann, S. Higher-order organization by mesoscale self-assembly and transformation of hybrid nanostructures. *Angewandte Chemie-International Edition* **2003,** *42*, 2350-2365, https://doi.org/10.1002/anie.200200562.
35. Colfen, H.; Antonietti, M. Mesocrystals: Inorganic superstructures made by highly parallel crystallization and controlled alignment. *Angewandte Chemie-International Edition* **2005**, *44*, 5576-5591, https://doi.org/10.1002/anie.200500496.
36. Yu, S.H.; Colfen, H.; Tauer, K.; Antonietti M. Tectonic arrangement of BaCO3 nanocrystals into helices induced by a racemic block copolymer. *Nature Materials* **2005,** *4*, 51-55, https://doi.org/10.1038/nmat1268.
37. Song, R. Q.; Colfen, H. Mesocrystals-ordered nanoparticle superstructures. *Advanced Materials* **2010,** *22*, 1301-1330, https://doi.org/10.1002/adma.200901365.
38. Colfen, H.; Antonietti, M. *Mesocrystals and nonclassical crystallization*. 2008, John Wiley & Sons, Ltd.
39. Kanamura, K.; Koizumi, S.H.; Dokko, K.R. Hydrothermal synthesis of LiFePO4 as a cathode material for lithium batteries. *Journal of Materials Science* **2008**, *43*, 2138-2142, http://dx.doi.org/10.1007/s10853-007-2011-1.
40. Mollaamin, F.; Monajjemi, M. DFT outlook of solvent effect on function of nano bioorganic drugs. *Physics and Chemistry of Liquids* **2012**, *50*, 596-604, https://doi.org/10.1080/00319104.2011.646444.
41. Mollaamin, F.; Gharibe, S.; Monajjemi, M. Synthesis of various nano and micro ZnSe morphologies by using hydrothermal method. *International Journal of Physical Sciences* **2011**, *6*, 1496-1500.
42. Mahdavian, L.; Monajjemi, M.; Mangkorntong, N. Sensor response to alcohol and chemical mechanism of carbon nanotube gas sensors. *Fullerenes Nanotubes and Carbon Nanostructures* **2009,** *17*, 484-495, https://doi.org/10.1080/15363830903130044.
43. Monajjemi, M.; Najafpour, J. Charge density discrepancy between NBO and QTAIM in single-wall armchair carbon nanotubes. *Fullerenes Nanotubes and Carbon Nano structures* **2014,** *22*, 575-594, https://doi.org/10.1080/1536383X.2012.702161.
44. Monajjemi, M.; Hosseini, M.S. Non bonded interaction of B16 N16 nano ring with copper cations in point of crystal fields. *Journal of Computational and Theoretical Nanoscience* **2013**, *10*, 2473-2477, https://doi.org/10.1166/jctn.2013.3233.
45. Monajjemi, M.; Mahdavian, L.; Mollaamin, F. Characterization of nanocrystalline silicon germanium film and nanotube in adsorption gas by Monte Carlo and Langevin dynamic simulation. *Bulletin of the Chemical Society of Ethiopia* **2008**, *22,* 277-286, https://doi.org/10.4314/bcse.v22i2.61299.
46. Lee, V.S.; Nimmanpipug, P.; Mollaamin, F.; Thanasanvorakun, S.; Monajjemi, M. Investigation of single wall carbon nanotubes electrical properties and normal mode analysis: Dielectric effects. *Russian Journal of Physical Chemistry A* **2009**, *83*, 2288-2296, https://doi.org/10.1134/S0036024409130184.
47. Mollaamin, F.; Najafpour, J.; Ghadami, S.; Akrami, M.S.; Monajjemi, M. The electromagnetic feature of B N H (x = 0, 4, 8, 12, 16, and 20) nano rings:Quantum theory of atoms in molecules/NMR approach. *Journal of Computational and Theoretical Nanoscience* **2014**, *11*, 1290-1298, https://doi.org/10.1166/jctn.2014.3495.
48. Monajjemi, M.; Mahdavian, L.; Mollaamin, F.; Honarparvar, B. Thermodynamic investigation of enolketo tautomerism for alcohol sensors based on carbon nanotubes as chemical sensors. *Fullerenes Nanotubes and Carbon Nanostructures* **2010**, *18*, 45-55, https://doi.org/10.1080/15363830903291564.
49. Monajjemi, M.; Ghiasi, R.; Seyed Sadjadi, M.A. Metalstabilized rare tautomers: N4 metalated cytosine (M = Li , Na , K , Rb and Cs), theoretical views. *Applied Organometallic Chemistry* **2003**, *17,* 635-640, https://doi.org/10.1002/aoc.469.
50. Ilkhani, A.R.; Monajjemi, M. The pseudo Jahn-Teller effect of puckering in pentatomic unsaturated rings C AE , A=N, P, As, E=H, F, Cl. *Computational and Theoretical Chemistry* **2015**, *1074*, 19-25, http://dx.doi.org/10.1016%2Fj.comptc.2015.10.006.
51. Monajjemi, M. Non-covalent attraction of B N and repulsion of B N in the B N ring: a quantum rotatory due to an external field. *Theoretical Chemistry Accounts* **2015,** *134*, 1-22, https://doi.org/10.1007/s00214-015-1668-9.
52. Monajjemi, M.; Naderi, F.;Mollaamin, F.; Khaleghian, M. Drug design outlook by calculation of second virial coefficient as a nano study. *Journal of the Mexican Chemical Society* **2012,** *56*, 207-211, https://doi.org/10.29356/jmcs.v56i2.323.
53. Monajjemi, M.; Bagheri, S.; Moosavi, M.S. Symmetry breaking of B2N(-,0,+): An aspect of the electric potential and atomic charges. *Molecules* **2015,** *20*, 21636-21657. https://doi.org/10.3390/molecules201219769.
54. Monajjemi, M.; Mohammadian,N.T. S-NICS: An aromaticity criterion for nano molecules. *Journal of Computational and Theoretical Nanoscience* **2015***, 12*, 4895-4914, https://doi.org/10.1166/jctn.2015.4458.
55. Monajjemi, M.; Ketabi, S.; Hashemian, Z.M.; Amiri, A. Simulation of DNA bases in water: Comparison of the Monte Carlo algorithm with molecular mechanics force fields. *Biochemistry (Moscow)* **2006,** *71 (SUPPL. 1),* S1-S8, https://doi.org/10.1134/s0006297906130013.
56. Monajjemi, M.; Lee, V.S.; Khaleghian, M.; Honarparvar, B.; Mollaamin, F. Theoretical Description of Electromagnetic Nonbonded Interactions of Radical, Cationic, and Anionic NH2BHNBHNH2 Inside of the B18N18 Nanoring. *J. Phys. Chem C* **2010**, *114*, 15315, https://doi.org/10.1021/jp104274z.
57. Monajjemi, M.; Boggs, J.E. A New Generation of BnNn Rings as a Supplement to Boron Nitride Tubes and Cages. *J. Phys. Chem. A* **2013**, *117*, 1670-1684, http://dx.doi.org/10.1021/jp312073q.
58. Monajjemi, M. Non bonded interaction between BnNn (stator) and BN B (rotor) systems: A quantum rotation in IR region. *Chemical Physics* **2013**, *425*, 29-45, https://doi.org/10.1016/j.chemphys.2013.07.014.
59. Monajjemi, M.; Robert, W.J.; Boggs, J.E. NMR contour maps as a new parameter of carboxyl's OH groups in amino acids recognition: A reason of tRNA–amino acid conjugation. *Chemical Physics* **2014**, *433*, 1-11, https://doi.org/10.1016/j.chemphys.2014.01.017.
60. Monajjemi, M. Quantum investigation of non-bonded interaction between the B15N15 ring and BH2NBH2 (radical, cation, and anion) systems: a nano molecularmotor. *Struct Chem* **2012,** *23*, 551–580, http://dx.doi.org/10.1007/s11224-011-9895-8.
61. Monajjemi, M. Metal-doped graphene layers composed with boron nitride–graphene as an insulator: a nano-capacitor. *Journal of Molecular Modeling* **2014**, *20*, 2507, https://doi.org/10.1007/s00894-014-2507-y.

62. Monajjemi M. Graphene/(h-BN)*n*/X-doped raphene as anode material in lithium ion batteries (X = Li, Be, B AND N). *Macedonian Journal of Chemistry and Chemical Engineering* **2017**, *36*, 101–118, http://dx.doi.org/10.20450/mjcce.2017.1134.
63. Monajjemi, M. Cell membrane causes the lipid bilayers to behave as variable capacitors: A resonance with self-induction of helical proteins. *Biophysical Chemistry* **2015**, *207*, 114-127, https://doi.org/10.1016/j.bpc.2015.10.003.
64. Monajjemi, M. Study of CD5+ Ions and Deuterated Variants (CHxD(5-x)+): An Artefactual Rotation. *Russian Journal of Physical Chemistry a* **2018,** *92***,** 2215-2226. https://doi.org/10.1134/S0036024418110286.
65. Monajjemi, M. Liquid-phase exfoliation (LPE) of graphite towards graphene: An ab initio study. *Journal of Molecular Liquids* **2017**, *230*, 461–472, https://doi.org/10.1016/j.molliq.2017.01.044.
66. Jalilian, H.; Monajjemi, M. Capacitor simulation including of X-doped graphene (X = Li, Be, B) as two electrodes and (hBN)m (m = 1–4) as the insulator. *Japanese Journal of Applied Physics* **2015**, *54,* 085101-7. http://dx.doi.org/10.7567/JJAP.54.085101.
67. Ardalan, T.; Ardalan, P.; Monajjemi, M. Nano theoretical study of a C 16 cluster as a novel material for vitamin C carrier. *Fullerenes Nanotubes and Carbon Nanostructures* **2014**, *22*, 687-708, https://doi.org/10.1080/1536383X.2012.717561.
68. Monajjemi, M.; Honarparvar, B.; Nasseri, S.M.; Khaleghian, M. NQR and NMR study of hydrogen bonding interactions in anhydrous and monohydrated guanine cluster model: A computational study, *Journal of structural chemistry* , **2009,** 50(1),67-77, https://doi.org/10.1007/s10947-009-0009-z.
69.Monajjemi,M.; Aghaei,H.; Naderi,F, Thermodynamic study of interaction of TSPP, CoTsPc, and FeTsPc with calf thymus DNA *Biochemistry(Moscow)*,**2007**, 72(6),652-657
70. Monajjemi,M.; Farahani,N.;Mollaamin,F.; Thermodynamic study of solvent effects on nanostructures: Phosphatidylserine and phosphatidylinositol membranes, Physics and Chemistry of Liquids ,**2012,** 50(2), 161-172, https://doi.org/10.1080/00319104.2010.527842.
71. Monajjemi, M.; Ahmadianarog, M.; Carbon nanotube as a deliver for sulforaphane in Broccoli vegetable in point of nuclear magnetic resonance and natural bond orbital specifications, Journal of Computational and Theoretical Nanoscience, **2014,** 11(6), 1465-1471, https://doi.org/10.1166/jctn.2014.3519.
72. Phm, T.T.; Monajjemi, M.; Dang, C. M., Fabrication of lithium-ion batteries based on various LiNi1–*x*Co*x*O2 cathode materials. *Int. J. Nanotechnol.* **2018***, 15*, 925-935, https://doi.org/10.1504/IJNT.2018.099932.
73. Monajjemi, M.; Dang, C.M.; Alihosseini, A.; Mollaamin, F. Designing BN sheets of X-G//(h-BN)n//X-G (X = B, N) and GO/h-BN/GO structures for based anodes material to improve the performance of lithium-ion batteries. *Int. J. Nanotechnology* **2018***, 15*, 819-844, https://dx.doi.org/10.1504/IJNT.2018.099925.
74. Thi, L.C.M.; Blanc, E.F.; Monajjemi, M.; Dang, C.M. Theoretical and experimental simulation of inkjet printing process: investigation of physical parameters of a droplet. *Int. J. Nanotechnol* **2018***, 15,* 845-857, https://doi.org/10.1504/IJNT.2018.099926.
75. Lu, T.; Chen, F. Multiwfn: A Multifunctional Wavefunction Analyzer. *J. Comp. Chem*. **2012**, *33*, 580-592, https://doi.org/10.1002/jcc.22885.

6. ACKNOWLEDGEMENTS

This research is funded by Vietnam National University – Ho Chi Minh city (VNU-HCM) under the grant number TX2020-32-01.